PCCP

PAPER

View Article Online
View Journal | View Issue



Cite this: *Phys. Chem. Chem. Phys.*, 2025, **27**, 24726

# Impact of cyclacene size on their electronically excited singlet states

Abdollah Omran, Divanshu Gupta and Holger F. Bettinger *

Received 30th May 2025,
Accepted 29th October 2025

DOI: 10.1039/d5cp02050f

rsc.li/pccp

Cyclacenes are cyclic analogs of acenes consisting of linearly fused benzene rings rolled into a cylindrical shape. Despite extensive theoretical investigations, their experimental synthesis remains challenging. This study employs the high-level NEVPT2-CASSCF computational method to explore the electronic excitation spectra of [*n*]-cyclacenes (*n* = 5–12). Our results reveal an oscillation in electronic properties, with even-*n* cyclacenes exhibiting strong electronic transitions in the visible range, while odd-*n* cyclacenes generally lack such features until *n* = 11. Additionally, the HOMO–LUMO transition in odd-*n* cyclacenes occurs at higher energies with greater intensity than in even-*n* counterparts. These findings provide crucial insights into the optical characteristics of cyclacenes and will guide future experimental identification efforts.



## 1. Introduction

Cyclacenes, proposed for the first time by Heilbronner in 1954,[1] are the cyclic version of acenes and consist of linearly fused benzene rings rolled up into a cylindrical form (Fig. 1). Cyclacenes are molecular sections of zig-zag carbon nanotubes with hydrogen atoms saturating the otherwise dangling bonds. Despite significant attempts over many decades, cyclacenes could not be synthesized employing conventional organic chemistry methods or on-surface synthesis, as summarized in a number of reviews.[2–7] This is most likely due to the high strain of the cyclacenes and their polyradical character that results from their acene-like topology.[8–15] However, laser irradiation under mass spectrometry conditions was reported by Wang and co-workers to result in the formation of a species with the molecular mass of [8]-cyclacene.[16]

Optical spectroscopy has played a crucial role in identifying larger acenes,[17–21] and it is expected to likewise enable the characterization of the yet unknown cyclacenes. Lacking experimental data, the current knowledge on cyclacenes is derived from theoretical investigations. Initial semiempirical investigations summarized by Türker and Gümüş[2] were followed by DFT and wavefunction analyses of their geometric and electronic structure, their aromaticity, as well as their reactivity.[8–15,22–30] It is expected that cyclacenes have an interesting electronic structure[31] related to acenes, which are well studied because of their potential use as active components in organic electronics.[32–42] Similar to larger acenes,[43,44] cyclacenes have an "open-shell" singlet ground state, *i.e.*, the closed-shell DFT description shows a triplet instability that suggests the existence of an antiferromagnetic coupling and polyradicaloid character in the ground state.[8–12]

Various DFT studies agree that the structure of [*n*]-cyclacenes is of $D_{nh}$ point group symmetry.[8,9,22–25] The bond lengths of all zig-zag edge bonds and all rung bonds, respectively, are thus identical. In contrast to acenes that have a single Clar sextet,[45,46] cyclacenes have no Clar sextet at all.[47] They can thus be considered as two polyacetylene chains, or two [2*n*]-trannulenes,[48] joined by rung bonds.[2,47]

Properties of smaller [*n*]-cyclacenes, such as the total energy of π-electrons $E_\pi$, HOMO–LUMO and singlet–triplet energy gap, show an even-*n*/odd-*n* oscillation.[10,12,13,49,50] Similar even–odd dependence was also observed for aromaticity based on magnetic criteria[22,26] and the energies of dimerization.[29] It was explained by the cryptoannulenic effect,[2,47] which ascribes aromatic or antiaromatic character to the polyacetylenic [2*n*]-trannulene building blocks of [*n*]-cyclacenes.[22,26]

The even–odd oscillation of the singlet–triplet energy gaps suggests that also the energies of excited states in the singlet manifold not only depend on the overall size of the system, but also on the nature of *n*. Even-*n* cyclacenes may thus have different absorption spectra than odd-*n* cyclacenes. This would be contrasting the optical properties of acenes that are known undergo continuous bathochromic shifts of absorption bands with increasing system size.[17–19,51] Acenes have typically three dominating relevant electronic transitions in the UV/vis spectrum, termed $^1B_b$ or β band (high intensity), $^1L_b$ or α band (weak intensity) and $^1L_a$ or p band (medium intensity) that is associated with the HOMO → LUMO transition. These characteristic bands, along with further strong bands that shift into

*Institut für Organische Chemie Eberhards Karls Universität Tübingen Auf der Morgenstelle 18, 72076 Tübingen, Germany.*
*E-mail: holger.bettinger@uni-tuebingen.de*

 

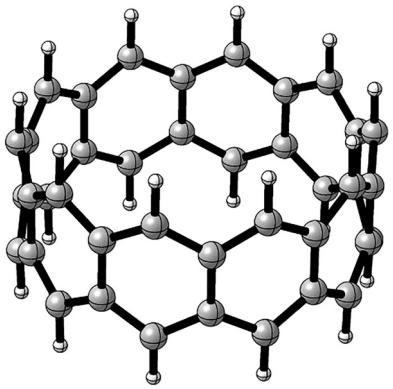

Fig. 1 Structure of [*n*]-cyclacene, *n* = 10.

the UV/vis region, allowed the identification of acenes.[17–21,51] Previous matrix isolation experiments elucidated the optical properties of large acenes up to undecacene and have extrapolated an optical gap associated with the HOMO → LUMO transition of 1.2 eV for infinitely large polyacene.[19] The absorption spectra were computed and analyzed using DFT/MRCI computations.[19,52,53]

Previous investigations of the excited electronic states of [*n*]-cyclacenes are limited to a recent study by Negri and coworkers.[14] The authors focused on the relative energies of the lowest energy $L_a$ state and the doubly excited state, a ''dark'' state in conventional optical spectroscopy, of even-*n* cyclacenes (*n* = 6, 8, 10, 12) using TD-DFT, TD-UDFT, SF-TDDFT, DFT/MRCI, and NEVPT2-CASSCF (*n* = 6, 8 only).[14] They concluded that the $L_a$ state is lower in energy for *n* = 6, 8, but that the ''dark'' state becomes the lowest energy state for [10]-cyclacene.[14]

The purpose of this work is to investigate the optically allowed excited states of a series of [*n*]-cyclacenes (*n* = [5,12], with *n* ranging from 5 to 12) to unravel their electronic excitation spectrum in the singlet manifold depending on odd-*n* or even-*n* and diameters. Although cyclacenes are closely related to the acene linear analogues, already the Hückel MO model suggests considerable differences, as ''the odd and even members of the series follow rather different electronic structure patterns''.[12] Hence, it can be expected that the absorption spectra of cyclacenes differ from those of acenes. The study is motivated by providing qualitative predictions of the UV/vis spectra to assist future experimental identification of [*n*]-cyclacenes, *e.g.*, under matrix isolation conditions as performed earlier for large acenes.[17–21] Knowledge of the optical spectra beyond the $L_a$ state is essential for cryogenic matrix isolation experiments as this will not only allow the identification of [*n*]-cyclacenes, but it can also guide the choice of experimental targets.

## 2. Computational methods

All geometries of [*n*]-cyclacenes (*n* = [5,12], with *n* ranging from 5 to 12) were optimized using the B3LYP hybrid functional and the def2-SV(P) basis set.[54–56] Negri *et al.*[14] showed that the contribution of the structural relaxation to the energy difference between spin-restricted closed-shell (CS) and broken-symmetry (BS) treatments is negligible for cyclacenes. To avoid any spin-contamination issues that might plague the structures obtained from the BS-DFT treatment, we have chosen to use the CS geometries for subsequent single point computations. The geometry parameters are similar to previous studies, see SI (Tables S1 and S2 and Fig. S1 and S2).

The computation of the excited state energies was done using the multi-configuration complete active space self-consistent field (CASSCF) method combined with strongly contracted *n*-electron valence state perturbation theory (NEVPT2),[57–60] using the RIJK[61,62] approximation. The def2-TZVP basis set, along with the recommended fitting basis set was employed.[56,63] The computations were done within the largest Abelian group of $D_{nh}$, *i.e.*, $D_{2h}$ for even-*n* (*n* = 6, 8, 10, 12) and $C_{2v}$ for odd-*n* cyclacenes (*n* = 5, 7, 9, 11). We investigated excitations from the ground state $^1A_g/^1A_1$ ($D_{2h}/C_{2v}$) to the first ten electronically excited states of each irreducible representation $B_{1u}$, $B_{2u}$, $B_{3u}/A_1$, $B_1$, $B_2$. These correspond to electric dipole allowed transitions that are expected to be relevant for the experimental identification of cyclacenes by optical spectroscopy.

The active space for the CASSCF computations was chosen using natural orbitals (NO) obtained from preliminary RI-MP2 runs. The molecular orbital energies and shapes are available in the SI (Tables S3 and S4 and Fig. S4–S11). To investigate the impact of the active space size (*k*, *l*; *k* = number of electrons, *l* = number of orbitals), this was varied from (8,8), (12,12) to (16,15) for [6]-cyclacene (Tables S5–S7). As the excited state energies and oscillator strengths do not vary qualitatively with active space size, we have chosen the (12,12) space for all cyclacenes reported in the manuscript. The full set of the excited state computations are available in the SI (Tables S5–S10) for even-*n* and Tables S15–S18 for the odd-*n* cyclacenes. The computations were performed using the Orca 5.0.4 program.[64–66]

## 3. Results and discussion

### 3.1. Molecular orbital energy diagrams

The molecular orbital energies that we obtained for the cyclacenes studied using CASSCF (Fig. 2) qualitatively follow the results reported by Pérez-Guardiola *et al.*[12] who have analyzed the molecular orbital energies around the Fermi level for even-*n* and odd-*n* cyclacenes. For odd-*n* cyclacenes the molecular orbitals come in degenerate pairs within the Hückel approximation.[12] Even-*n* cyclacenes have a set of degenerate frontier molecular orbitals occupied by two electrons.[12] This degeneracy is lifted by 1,4 transannular interactions resulting in a unique set of highest occupied molecular orbital (HOMO) and lowest occupied molecular orbital (LUMO) levels for even-*n* cyclacenes (Fig. 2).[12] For convenience, we label the HOMO, HOMO−1, HOMO−2, *etc.* as 1, 2, 3 and lowest unoccupied LUMO, LUMO+1, LUMO+2, ... as 1′, 2′, 3′, .... Thus, for even-*n*

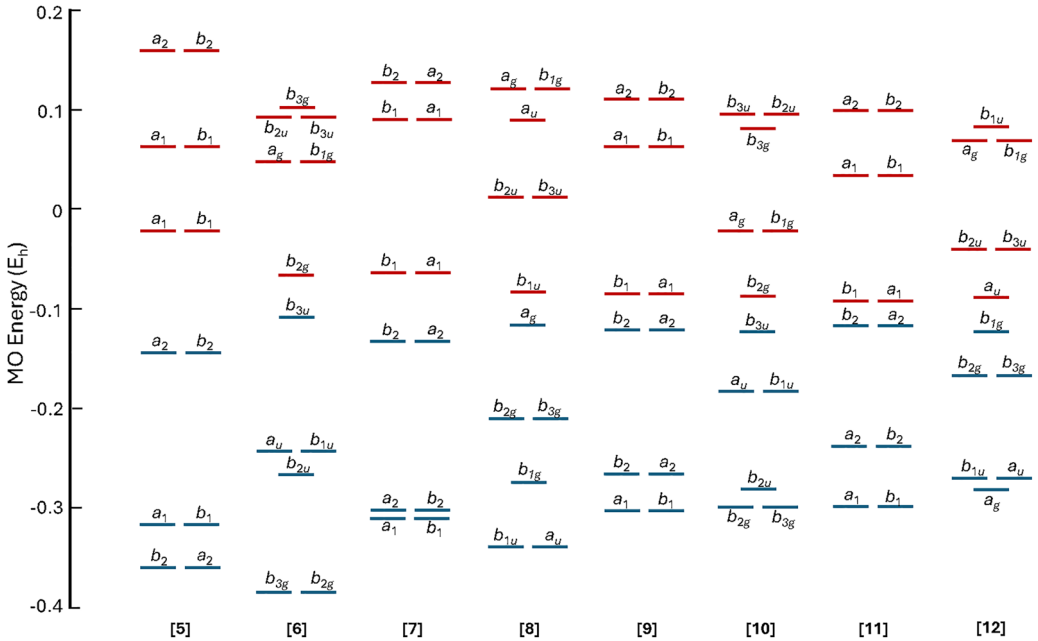


Fig. 2 The molecular orbital diagrams ($E$ in $E_h$) of [$n$]-cyclacenes ($n$ = [5,12]) in the range from (HOMO−5) to (LUMO+5) as computed at the CASSCF(12,12)/def2-TZVP level of theory. Occupied and vacant MO are in blue and red, respectively. Symmetry labels given are for $D_{2h}$ (even $n$) and $C_{2v}$ (odd $n$) point groups.

cyclacenes ($n$ = 6, 8, 10, and 12), the doubly degenerate orbitals are generally 5/4, 3/2 followed by 2′/3′ and 4′/5′, while 1 and 1′ are not degenerate (Fig. 2). In contrast, for odd-$n$ cyclacenes ($n$ = 5, 7, 9, and 11), the doubly degenerate orbitals are usually 6/5, 4/3, 2/1, followed by 1′/2′, 3′/4′, and 5′/6′ (Fig. 2). Even-$n$ cyclacenes have a smaller HOMO–LUMO gap than the preceding and succeeding odd cyclacenes, especially for smaller n numbers (see, SI Table S4). The difference in gap size and the gap itself decrease as the cyclacene size increases.

Cyclacenes are alternant polycyclic aromatic hydrocarbons and therefore the approximate pairing of molecular orbitals with respect to their energy levels is observable for the larger members. For example, in [8]-cyclacene, the MO energy difference $\Delta\varepsilon$ between (H−1), (H−2), and LUMO and between (L+1), (L+2) and HOMO are equal (see Fig. S3 in SI for a more detailed analysis).

# 4. Excited singlet states of cyclacenes

## 4.1. Symmetry considerations

The structures of $n$-cyclacenes are of $D_{nh}$ symmetry. For even-$n$ systems, the electric dipole allowed electronic transitions fall into the $A_{2u}$ and $E_{1u}$ irreducible representations. The computations were performed using the largest Abelian subgroup $D_{2h}$ of the $D_{nh}$ ($n$ even) groups. In $D_{2h}$, the electric dipole allowed electronic transitions are in the $B_{1u}$, $B_{2u}$, and $B_{3u}$ irreducible representations. The correlation of $D_{nh}$ to $D_{2h}$ shows that $E_{1u}$ corresponds to $B_{2u}$ + $B_{3u}$ and $A_{2u}$ to $B_{1u}$.[67]

For odd-$n$ systems the electric dipole allowed electronic transitions are $A_2''$ and $E_1'$, while in the largest Abelian subgroup $C_{2v}$, they are $A_1$, $B_1$, and $B_2$. The correlation of $D_{nh}$ to $C_{2v}$ shows that $A_2''$ corresponds to $B_2$ and $E_1'$ to $A_1$ + $B_1$.[67] Note that any computation of the electric dipole allowed electronic transitions in $D_{2h}$ or $C_{2v}$ will also include states that are electric dipole forbidden in the higher symmetry point groups $D_{nh}$. For this reason, we only include electronic transitions with oscillator strengths $f > 0.001$ in the following discussion. All computed excited states, irrespective of their oscillator strengths, are available in the SI (Tables S6–S15).

In the following, we analyze the excitations of the even-$n$ and odd-$n$ cyclacenes first in the highest possible point group and deduce the consequences of a lowering in symmetry to the computational point groups. For even-$n$ cyclacenes we analyze the consequences of symmetry lowering for [8]-cyclacene in the $D_{8h}$ point group, in which excitations from the ground state $A_{1g}$ to $A_{2u}$ and $E_{1u}$ states are electric dipole allowed. The HOMO and LUMO are $4b_{1g}$ and $4b_{2u}$, respectively, and the direct product, $b_{1g} \times b_{2u} = a_{2u}$, shows that the HOMO–LUMO transition from the ground state $A_{1g}$ to $A_{2u}$ is electric dipole allowed. In the computational point group $D_{2h}$, the HOMO–LUMO transition corresponds to an $A_{1g} \rightarrow B_{1u}$ excitation.

For odd-$n$ cyclacenes we focus on [7]-cyclacene that has $D_{7h}$ point group. Electronic transitions from the ground state $A_1'$ are electric dipole allowed to $A_2''$ and $E_1'$ states. The HOMO and LUMO are $6e_3''$ and $8e_3'$, respectively. The direct product, $e_3'' \times e_3' = a_1'' \oplus a_2'' \oplus e_1''$, shows that the HOMO–LUMO excitation is allowed from the ground state $A_1'$ to $A_2''$, but forbidden for $A_1' \rightarrow A_2''$ and $A_1' \rightarrow E_1''$. In the computational point group $C_{2v}$, the $A_2''$ state is $B_2$, while $A_2''$ and $E_1''$ correspond to $A_2$ and ($A_2$ + $B_2$), respectively. Hence, we expect the HOMO–LUMO transition to be represented by four distinct excited states, $B_2$, $A_2$, $A_2$, $B_2$,

 

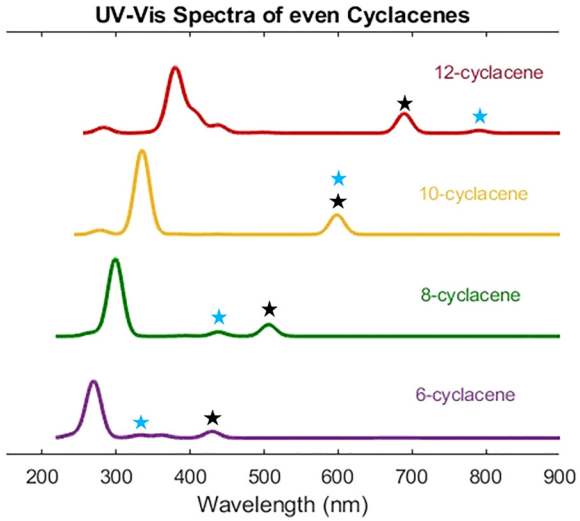


Fig. 3 Absorption spectra of even-*n* cyclacenes (6–12) as computed at the NEVPT2/def2-TZVP level of theory. The spectra were derived from the computed transition energies by Gaussian broadening with $\sigma$ = 10. The blue and black stars correspond to the $B_{1u}$ and $B_{2u}/B_{3u}$ excited states, respectively, which appear in the visible light range with an intensity $f >$ 0.15 in even-*n* cyclacenes.

with one $B_2$ and one $A_2$ state (for simplicity, we only computed the $B_2$ states) being degenerate. The pairwise degeneracy of the frontier orbitals of odd-*n* cyclacenes has a pronounced impact on the electronic excited states compared to linear acenes, where these orbitals are not degenerate and electronic transitions among those four orbitals give rise to the four well-known states of polycyclic aromatic hydrocarbons, namely $L_a$, $L_b$, $B_a$, and $B_b$.[68] Thus, it is expected (and confirmed by our computations, *vide infra*) that energetically low-lying electronic transitions are forbidden for odd-*n* cyclacenes, except for a transition akin to $^1A \rightarrow {}^1L_a$ in acenes.

### 4.2. Impact of active space size

The choice of the active space in CASSCF computations is not trivial if molecules in a homologous series are investigated. Larger systems are expected to require a larger active space for a balanced treatment. However, larger active spaces will result in a larger density of excited states, as we will show below for [6]-cyclacene. For [6]-cyclacene the smallest active space investigated, (8,8)-NEVPT2 (Table S5), finds four $E_{1u}$ states and four $A_{2u}$ states within the energy range of 1115 nm–280 nm with the 4 $E_{1u}$ state at 280 nm having a very large oscillator strength of $f$ = 3.67. Note that these energy ranges cover the NIR-UV/Vis range that is typically easily accessible experimentally. Increasing the active space to (12,12) results in a significantly larger number of states in the energy range up to 280 nm (Table S6), in particular several forbidden states now appear additionally in this energy range. The most intense 4 $E_{1u}$ state is at 296 nm with $f$ = 3.241. With the yet larger (16,15) active space the density of states increases further (Table S7), and the strongly absorbing state is no longer among the computed states as many forbidden states (the forbidden states $B_{2u}$, $B_{3u}$, $E_{2u}$ in $D_{6h}$

**Table 1** Singlet state excitation wavelengths ($\lambda$, in nm), oscillator strengths, dominant contributions to the electronic wavefunctions and their weights as computed at the CAS(12,12)-NEVPT2/def2-TZVP level of theory[a]

| | | 6cyc | | 8cyc | | 10cyc | | 12cyc | |
|---|---|---|---|---|---|---|---|---|---|
| State | Sym. species | $\lambda$/nm, $f$ | Orbs., weight | $\lambda$/nm, $f$ | Orbs., weight | $\lambda$/nm, $f$ | Orbs., weight | $\lambda$/nm, $f$ | Orbs., weight |
| $^1L_a$ | $B_{1u}$ | 1304, 0.010 | 1 → 1′ (0.80) | 1415, 0.009 | 1 → 1′ (0.79) | 1476, 0.002 | 1 → 1′(0.70) | 1475, 0.002 | 1 → 1′(0.53) |
| $^1L_b$ | $B_{2u}$ + $B_{3u}$ | 680, 0.008 | 1 → 2′/3′ (0.45) | 851, 0.004 | 1 → 2′/3′ (0.38) | 1116, 0.000 | 1 → 2′/3′(0.35) | 1432, 0.000 | 1 → 2′/3′(0.33) |
| | | | 2/3 → 1′ (0.28) | | 2/3 → 1′ (0.36) | | 2/3 → 1′(0.34) | | 2/3 → 1′(0.31) |
| $S_k$ | $B_{1u}$ | 363, 0.006 | 2 → 2′ (0.23) | 491, 0.000 | 2 → 2′ (0.36) | 680, 0.000 | 2 → 2′(0.35) | 922, 0.000 | 2 → 2′(0.33) |
| | | | 3 → 3′ (0.46) | | 3 → 3′(0.36) | | 3 → 3′(0.35) | | 3 → 3′(0.33) |
| $^1B_b$ | $B_{2u}$ + $B_{3u}$ | 429, 0.375 | 1 → 2′/3′ (0.19) | 506, 0.696 | 1 → 2′/3′(0.28) | 599, 0.960 | 1 → 2′/3′(0.28) | 689, 1.168 | 1 → 2′/3′(0.26) |
| | | | 2/3 → 1′ (0.38) | | 2/3 → 1′(0.30) | | 2/3 → 1′(0.27) | | 2/3 → 1′(0.24) |
| $S_l$ | $B_{1u}$ | 332, 0.164 | 2 → 2′ (0.40) | 438, 0.254 | 2 → 2′ (0.30) | 597, 0.226 | 2 → 2′ (0.25) | 791, 0.156 | 2/3 → 2′/3′ (0.3) |
| | | | 3 → 3′ (0.18) | | 3 → 3′ (0.30) | | 3 → 3′ (0.26) | | 1 → 1′ (0.26) |
| $S_m$ | $B_{2u}$ + $B_{3u}$ | 360, 0.159 | 4 → 2′/3′ (0.36) | 393, 0.032 | 4 → 2′/3′(0.35) | 436, 0.016 | 4 → 2′/3′(0.33) | 574, 0.000 | 4 → 2′/3′(0.31) |
| | | | 2/3 → 6′ (0.26) | | 2/3 → 4′(0.30) | | 2/3 → 4′ (0.29) | | |
| $^1D_1$ | $B_{1u}$ | 468, 0.000 | 1,1 → 1′,5′ (0.70) | 364, 0.000 | 1,1 → 1′,5′ (0.50) | 387, 0.000 | 1,5 → 1′,1′ (0.31) | 458, 0.000 | 1,5 → 1′,1′(0.34) |
| | | | | | | | 1,1 → 1′,5′ (0.19) | | 1,1 → 1′,5′(0.19) |
| $^1D_2$ | $B_{2u}$ + $B_{3u}$ | 270, 3.241 | 2,3 → 6′,6′(0.33) | 299, 4.602 | 2,3 → 4′,4′(0.28) | 335, 5.301 | 2,3 → 4′,4′(0.26) | 380, 2.846 | 2,3 → 6′,6′(0.13) |
| | | | 4,4 → 2′,3′(0.12) | | 4,4 → 2′,3′(0.19) | | 4,4 → 2′,3′(0.21) | | 6 → 2′/3′(0.10) |

[a] The following notation is used: n/m indicates that excitation involves orbitals n or m; n, m indicates that excitation involves orbitals n and m.

are transforming to $B_{2u}$, $B_{1u}$ and $B_{1u}$ + $A_u$ in $D_{2h}$, respectively) are now also picked up in the CASSCF solution. We expect that an increase in the number of states considered for the (16,15) active space would bring back the bright state into the considered energy range. We have chosen the (12,12) active space for all the systems investigated as a compromise as we expect that the essential features of the absorption spectra are reproduced with this method.

### 4.3. Even-*n* cyclacenes

The overall appearance of the electronic absorption spectra as obtained by the NEVPT2/def2-TZVP method for the even-*n* cyclacenes are graphically summarized in Fig. 3 (for Tables with all excited states and a more detailed discussion of

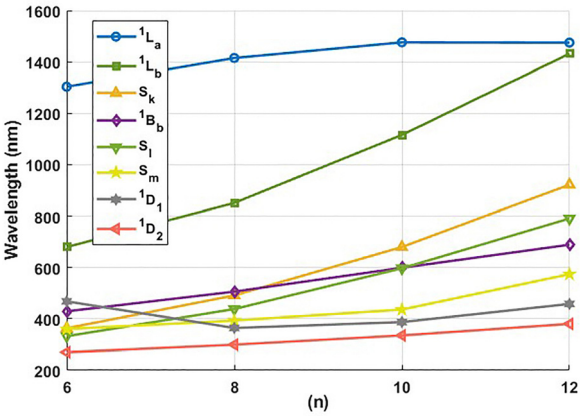


Fig. 4 Change of the excitation wavelength to selected excited states of even-*n* cyclacenes as computed at the NEVPT2/def2-TZVP level of theory. Lines to guide the eye.

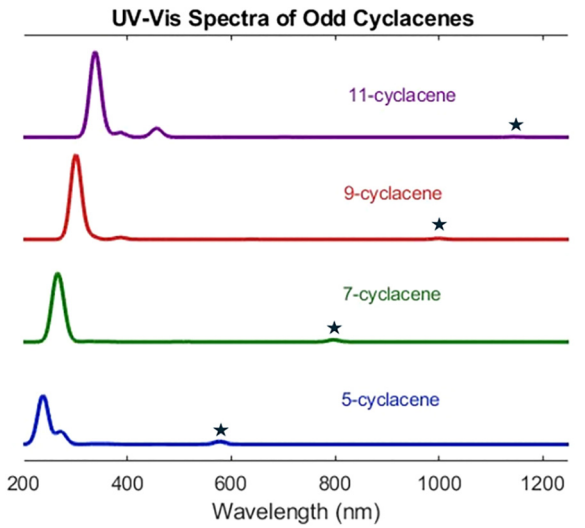


Fig. 5 Absorption spectra of odd-*n* cyclacenes (5–11) as computed at the NEVPT2/def2-TZVP level of theory. The stars mark the bands associated with the H → L transition. The spectra were derived from the computed transition energies and oscillator strengths by Gaussian broadening with $\sigma$ = 10.

Table 2 Singlet state excitation wavelengths ($\lambda$, in nm) and oscillator strengths for odd-*n* cyclacenes as computed at the CAS(12,12)-NEVPT2/def2-TZVP level of theory[a]

| | Sym. | 5cyc | | 7cyc | | 9cyc | | 11cyc | |
|---|---|---|---|---|---|---|---|---|---|
| State | species | $\lambda$/nm, $f$ | Orbs., weight | $\lambda$/nm, f | Orbs., weight | $\lambda$/nm, $f$ | Orbs., weight | $\lambda$/nm, $f$ | Orbs., weight |
| $^1L_a$ | $B_2$ | 578, 0.149 | 1-1′ (0.38) 2-2′ (0.38) | 797, 0.111 | 1-1′ (0.38) 2-2′ (0.38) | 999, 0.054 | 1-1′ (0.32) 2-2′ (0.32) | 1145, 0.021 | 1-1′ (0.25) 2-2′ (0.25) |
| $^1B_b$ | $A_1$ + $B_1$ | 240, 0.952 | $A_1$: 2-5′ (0.08) 1-6′ | 264, 2.700 | $A_1$: 2 → 5′ (0.06) $B_1$: 1 → 6′/$B_1$: 1 → 5′ (0.08)/2 → 6′ (0.07) | 301, 4.222 | $A_1$: 2 → 6′ (0.08) 1 → 5′/6 → 2′(0.06) 5 → 1′ $B_1$: 1 → 6′ (0.08) 2 → 5′/5 → 2′(0.06) 6 → 1′ | 337, 3.8 | $A_1$: 1,1,6-1′,1′,2′ 2,2,5-1,2′,2′ 1-5′/2-6′/1,1,2 → 1′,1′,6′/1,2,2 → 2′,2′,5′ (0.05). $B_1$: 1,1,5 → 1′,1′,2′/2,2,6 → 1′,2′,2′/1,1,2 → 1′,1′,5′/1,2,2 → 2′,2′,6′ (0.06)/1 → 6′ (0.05) 2 → 5′ |
| | | | $B_1$: 1,2-4′,4′(0.14) 1,2- 3′,3′(0.12) | | | | | | |

[a] The following notation is used: n/m indicates that excitation involves orbitals n or m; n, m indicates that excitation involves orbitals n and m.

individual [*n*]-cyclacenes, see SI). These computations show that even-*n* cyclacenes have very high intensity bands within the UV range that increase in intensity and shift bathochromically with increasing system size up to $n = 10$. For [12]-cyclacene, the high intensity peak is already shifted into the visible range and appears to be split, resulting in decreased peak height. An additional peak of considerable intensity appears in the visible range ($\lambda = 429$ nm for [6]-cyclacene, $\lambda = 689$ nm for [12]-cyclacene) that likewise shifts bathochromically and gains intensity ($f = 0.38$ to 1.18) with increasing size.

The excited electronic states that are most relevant for the appearance of the absorption spectra were analyzed in terms of electronic excitations (see Table 1). Due to the similarity of excitation patterns, we label states as in acenes. The lowest energy electric dipole allowed excited state is $1^1B_{1u}$ for all even-*n* cyclacenes that is due to excitation from HOMO to LUMO ($1 \rightarrow 1'$) and is thus labelled $^1L_a$. The transition dipole moments (see SI) are oriented along the n-fold rotational axes of the [*n*]-cyclacenes and thus these states resemble the short-axis polarized $^1L_a$ states of acenes. As observed for acenes, the oscillator strength decreases with increasing size.[53] It is remarkable that their absorption wavelengths are shifted towards the NIR range much more than that of similar sized acenes.[53] This is because for even-*n* cyclacenes the HOMO–LUMO energy gap is smaller than for acenes as it arises due to 1,4-transannular interaction as discussed above.[12]

Other relevant states of acenes, such as $^1L_b$, and $^1B_b$ can also be identified among even-*n* cyclacenes (Table 1). The $^1L_b$ states are of ($B_{2u}$ + $B_{3u}$) symmetry and their transition dipole moments are within the planes that dissect the cyclacenes through their rung bonds (*xy* plane). This resembles the long-axis polarization of acenes. The $^1L_b$ states arise from $H \rightarrow L+1$ and $H-1 \rightarrow L$ excitations and have small oscillator strengths.

As for acenes, $H \rightarrow L+1$ and $H-1 \rightarrow L$ excitations also give rise to the $^1B_b$ states. These are of ($B_{2u}$ + $B_{3u}$) symmetry, are polarized within the xy plane and have large oscillator strengths. As for $^1L_a$ and $^1L_b$, the excitation wavelengths are significantly longer than for acenes of similar size.[53] These strong absorptions in the visible range are expected to be very helpful for experimental identification of even-*n* cyclacenes.

For larger acenes, two-electron transitions could be identified that were labelled $^1D_1$ and $^1D_2$ previously.[53] While $^1D_1$ always had very small oscillator strength, $^1D_2$ acquired large oscillator strength once it was lower in energy than $^1B_b$.[53] The corresponding states of even-*n* cyclacenes also are dark ($^1D_1$, *n*-axis polarized) or very bright ($^1D_2$, polarized orthogonal to *n*-axis). The $^1D_2$ states have the highest oscillator strengths for any given even-*n* cyclacene, which is remarkable considering they are higher in energy than the $^1B_b$ states. This is an indication of the multiradical character of the ground state of these molecules as otherwise such formal two-electron excitations are expected to have very small oscillator strengths.

The evolution of the individual excited state wavelengths with cyclacene size is given in Fig. 4. It reveals that almost all of them shift bathochromically due to reduced orbital energy gaps (see Fig. 2), but not monotonically.

### 4.4. Odd-*n* cyclacenes

The overall appearance of the electronic absorption spectra as obtained by the NEVPT2/def2-TZVP method for the odd-*n* cyclacenes is graphically summarized in Fig. 5 (a more detailed discussion of individual [*n*]-cyclacenes is provided in the SI). These computations show that odd-*n* cyclacenes generally have much lower intensity bands within the UV/vis-NIR range than even-*n* cyclacenes. While the bands in the UV range have oscillator strengths of $f = 3$–5 and those in the visible range have around $f = 1$ for even-*n* cyclacenes, the values for odd-*n*

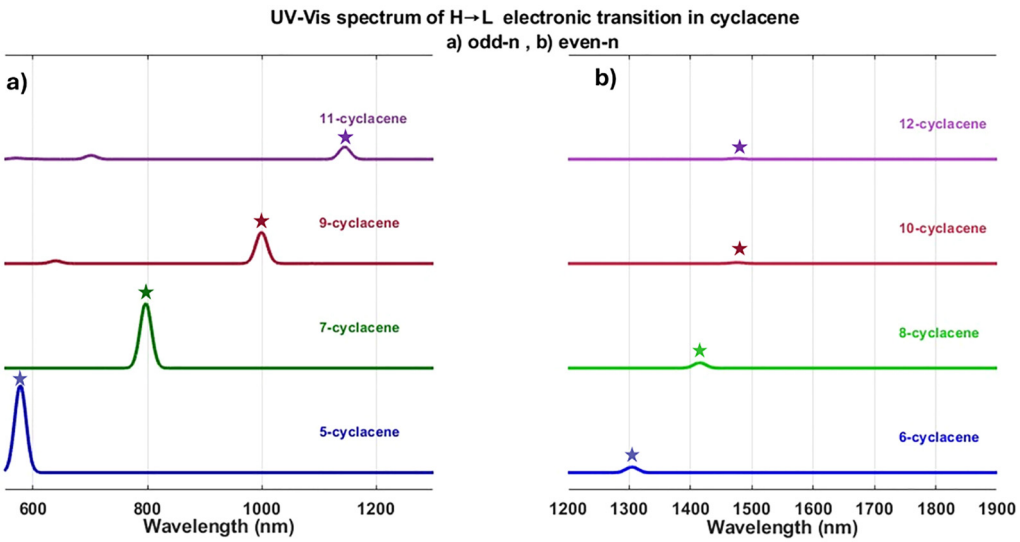


Fig. 6 HOMO–LUMO electronic transition in the absorption spectra of (a) odd-*n* (5–11) and (b) even-*n* cyclacenes (6–12) as computed at the NEVPT2/def2-TZVP level of theory. The spectra were derived from the computed transition energies by Gaussian broadening with $\sigma = 10$ and were normalized to the strongest signal of [5]-cyclacene.

cyclacenes are around $f$ = 0.5 and $f$ = 0.05, respectively. The bands in the visible range decrease in intensity and shift bathochromically with increasing system size. The difference in intensities will have profound impact on the potential identification of odd-$n$ cyclacenes by optical spectroscopy and its origin will be discussed below.

The $^1L_a$ states of odd-$n$ cyclacenes are of $B_2$ symmetry species and result from H → L excitation, as in even-$n$ cyclacenes and acenes (Table 2). The transition dipole moments are polarized along the $n$-fold rotational axis as in even-$n$ cyclacenes. The transition wavelengths are in a similar range as for the corresponding acenes, indicating that the HOMO–LUMO energy gaps are of similar size. As with acenes, the transition wavelengths evolve towards the NIR region with increasing size. Comparison of the absorption spectra in the wavelength range of the $^1L_a$ states reveal the significant differences of even-$n$ and odd-$n$ cyclacenes (Fig. 6). Note that the $^1L_a$ states are not the lowest energy excited states of odd-$n$ cyclacenes as there is an increasing number of dark states with increasing n (see the Tables S15–S18 in SI).

Almost all other states that have longer excitation wavelengths than $^1L_a$ have two-electron or even three-electron excitation character and as such have no resemble to the conventional acene excited states ($^1L_b$, $^1B_b$). As they also have very small oscillator strengths, we will not discuss them further. One excited state in the UV range stands out as having very high oscillator strengths. The major configuration, at least for [7]- and [9]-cyclacene, is due to H → L + 2/H−2 → L and transition dipole moment is polarized within the plane that bisects the molecule through the rung bonds. This state thus resembles $^1B_b$ and it falls into the same energy range as for acenes. Note that the weight of the H → L + 2/H−2 → L is rather small and further decreases for [5]- and [11]-cyclacenes, while two-electron and three-electron excitations, respectively, gain weight.

## 5. Conclusions

The computational investigation of the excited state energies of even-$n$ and odd-$n$ cyclacenes ranging from $n$ = [5,12] employing the NEVPT2 methods shows that the energy of all excited states decreases as $n$ increases in [$n$]-cyclacenes. The intensity for their electronic transition generally increases, except for the H → L transition, which follows the opposite trend. Even-$n$ cyclacenes exhibit excited states with strong intensity in the visible range, whereas small odd-$n$ cyclacenes do not. As the excited states shift to lower energies, a transition shifts into the visible range for [11]-cyclacene. The HOMO–LUMO transition occurs at a higher energy in odd-$n$ cyclacenes and has greater intensity compared to even-$n$ cyclacenes. The weight of the Aufbau principle electronic configuration in the ground state drops fast for odd-$n$ cyclacenes, and it is just 0.25 for [11]-cyclacene, but remains the leading configuration, while the weight of the electronic configuration where H−1, H, L, L+1 each contains one electron increases. This behavior suggests that the odd-$n$ cyclacenes have high polyradical character.

Optical spectroscopy was essential for the identification of the larger acenes,[17–21] and it is possible that the characterization of the yet unknown cyclacenes will also be facilitated by this spectroscopic method. The computational study reveals the excited electronic state manifold, which will be helpful for the experimental observation of cyclacenes and the assignment of spectra. The study also shows that the detection of odd-$n$ cyclacenes by optical spectroscopy in the presence of possibly unreacted (photo)precursors will be challenging as they lack characteristic strong absorption bands in the visible range.

## Conflicts of interest

The authors declare no conflict of interest.

## Data availability

The data supporting this article have been included as part of the supplementary information (SI). Supplementary information: discussion of structural parameters, molecular orbital energies and gaps, images of the molecular orbitals, all excited state energies and oscillator strengths, Cartesian coordinates. See DOI: **https://doi.org/10.1039/d5cp02050f**.

## Acknowledgements

This project has received funding from the European Research Council (ERC) under the European Union's HORIZON Europe ERC Synergy Grants action *via* the project Tackling the Cyclacene Challenge (TACY), grant agreement number 101071420-TACY-ERC-2022-SYG. The computations were performed on the BwForCluster JUSTUS2. The authors acknowledge support by the state of Baden-Württemberg through bwHPC and the German Research Foundation (DFG) through grant no. INST 40/575-1 FUGG (JUSTUS 2 cluster) for computation facilities.

## References

1 E. Heilbronner, *Helv. Chim. Acta*, 1954, **37**, 921–935.
2 L. Türker and S. Gümüş, *J. Mol. Struct. THEOCHEM*, 2004, **685**, 1–33.
3 R. Gleiter, B. Esser and S. C. Kornmayer, *Acc. Chem. Res.*, 2009, **42**, 1108–1116.
4 D. Eisenberg, R. Shenhar and M. Rabinovitz, *Chem. Soc. Rev.*, 2010, **39**, 2879–2890.
5 H. Chen and Q. Miao, *J. Phys. Org. Chem.*, 2020, **33**, e4145.
6 T.-H. Shi and M.-X. Wang, *CCS Chemistry*, 2021, **3**, 916–931.
7 Q.-H. Guo, Y. Qiu, M.-X. Wang and J. Fraser Stoddart, *Nat. Chem.*, 2021, **13**, 402–419.
8 Z. Chen, D. E. Jiang, X. Lu, H. F. Bettinger, S. Dai, P. V. Schleyer and K. N. Houk, *Org. Lett.*, 2007, **9**, 5449–5452.
9 D. Sadowsky, K. McNeill and C. J. Cramer, *Faraday Discuss.*, 2010, **145**, 507–521.
10 C.-S. Wu, P.-Y. Lee and J.-D. Chai, *Sci. Rep.*, 2016, **6**, 37249.

11 S. Battaglia, N. Faginas-Lago, D. Andrae, S. Evangelisti and T. Leininger, *J. Phys. Chem. A*, 2017, **121**, 3746–3756.
12 A. Pérez-Guardiola, M. E. Sandoval-Salinas, D. Casanova, E. San-Fabián, A. J. Pérez-Jiménez and J. C. Sancho-García, *Phys. Chem. Chem. Phys.*, 2018, **20**, 7112–7124.
13 D. Gupta, A. Omont and H. F. Bettinger, *Chem. – Eur. J.*, 2021, **27**, 4605–4616.
14 Y. Dai, J.-C. Sancho-García and F. Negri, *Chemistry*, 2023, **5**, 616–632.
15 Y. Segawa, A. Yagi, H. Ito and K. Itami, *Org. Lett.*, 2016, **18**, 1430–1433.
16 T.-H. Shi, Q.-H. Guo, S. Tong and M.-X. Wang, *J. Am. Chem. Soc.*, 2020, **142**, 4576–4580.
17 R. Mondal, B. K. Shah and D. C. Neckers, *J. Am. Chem. Soc.*, 2006, **128**, 9612–9613.
18 C. Tönshoff and H. F. Bettinger, *Angew. Chem., Int. Ed.*, 2010, **49**, 4125–4128.
19 B. Shen, J. Tatchen, E. Sanchez-Garcia and H. F. Bettinger, *Angew. Chem., Int. Ed.*, 2018, **57**, 10506–10509.
20 R. Mondal, C. Tönshoff, D. Khon, D. C. Neckers and H. F. Bettinger, *J. Am. Chem. Soc.*, 2009, **131**, 14281–14289.
21 H. F. Bettinger, R. Mondal and D. C. Neckers, *Chem. Commun.*, 2007, 5209–5211.
22 H. S. Choi and K. S. Kim, *Angew. Chem., Int. Ed.*, 1999, **38**, 2256–2258.
23 K. N. Houk, P. S. Lee and M. Nendel, *J. Org. Chem.*, 2001, **66**, 5517–5521.
24 S. Irle, A. Mews and K. Morokuma, *J. Phys. Chem. A*, 2002, **106**, 11973–11980.
25 K. P. Loh, S. W. Yang, J. M. Soon, H. Zhang and P. Wu, *J. Phys. Chem. A*, 2003, **107**, 5555–5560.
26 Q. Li, H.-L. Xu and Z.-M. Su, *New J. Chem.*, 2018, **42**, 1987–1994.
27 M. W. D. Hanson-Heine, D. M. Rogers, S. Woodward and J. D. Hirst, *J. Phys. Chem. Lett.*, 2020, **11**, 3769–3772.
28 M. W. D. Hanson-Heine and J. D. Hirst, *J. Phys. Chem. A*, 2020, **124**, 5408–5414.
29 A. Somani, D. Gupta and H. F. Bettinger, *J. Phys. Chem. A*, 2024, **128**, 6847–6852.
30 A. Somani, D. Gupta and H. F. Bettinger, *Chemistry*, 2025, **7**, 62.
31 B. Esser, *Phys. Chem. Chem. Phys.*, 2015, **17**, 7366–7372.
32 S. R. Würthner, *ChemPhysChem*, 2006, **7**, 793–797.
33 J. E. Anthony, *Chem. Rev.*, 2006, **106**, 5028–5048.
34 J. E. Anthony, *Angew. Chem.*, 2008, **47**, 452–483.
35 H. F. Bettinger, *Pure Appl. Chem.*, 2010, **82**(4), 905–915.
36 C. Tönshoff and H. F. Bettinger, *Chem. – Eur. J.*, 2021, **27**, 3193–3212.
37 H. F. Bettinger and C. Tönshoff, *Chem. Rec.*, 2015, **15**, 364–369.
38 C. Tönshoff and H. F. Bettinger, *Top. Curr. Chem.*, 2014, **349**, 1–30.
39 M. Bendikov, F. Wudl and D. F. Perepichka, *Chem. Rev.*, 2004, **104**, 4891–4945.
40 L. Lerena, R. Zuzak, S. Godlewski and A. M. Echavarren, *Chem. – Eur. J.*, 2024, **30**, e202402122.
41 K. J. Thorley and J. E. Anthony, *Isr. J. Chem.*, 2014, **54**, 642–649.
42 M. Watanabe, K.-Y. Chen, Y. J. Chang and T. J. Chow, *Acc. Chem. Res.*, 2013, **46**, 1606–1615.
43 M. Bendikov, H. M. Duong, K. Starkey, K. N. Houk, E. A. Carter and F. Wudl, *J. Am. Chem. Soc.*, 2004, **126**, 7416–7417.
44 M. Baldo, G. Piccitto, R. Pucci and P. Tomasello, *Phys. Lett.*, 1983, **95A**, 201–203.
45 E. Clar, *The Aromatic Sextet*, Wiley-Interscience, London, 1972.
46 M. Solà, *Front. Chem.*, 2013, **1**, 22.
47 L. Türker, *Polycyclic Aromat. Compd.*, 1994, **4**, 191–197.
48 A. A. Fokin, H. Jiao and P. V. R. Schleyer, *J. Am. Chem. Soc.*, 1998, **120**, 9364–9365.
49 L. Türker, *Turk. J. Chem.*, 1998, **22**, 109–114.
50 J.-M. André, B. Champagne, E. A. Perpète and M. Guillaume, *Int. J. Quantum Chem.*, 2001, **84**, 607–616.
51 N. Nijegorodov, V. Ramachandran and D. P. Winkoun, *Spectrochim. Acta A*, 1997, **53**, 1813–1824.
52 C. M. Marian and N. Gilka, *J. Chem. Theory Comput.*, 2008, **4**, 1501–1515.
53 H. F. Bettinger, C. Tönshoff, M. Doerr and E. Sanchez-Garcia, *J. Chem. Theory Comput.*, 2016, **12**, 305–312.
54 A. D. Becke, *J. Chem. Phys.*, 1993, **98**, 5648–5652.
55 C. Lee, W. Yang and R. G. Parr, *Phys. Rev. B: Condens. Matter Mater. Phys.*, 1988, **37**, 785–789.
56 F. Weigend and R. Ahlrichs, *Phys. Chem. Chem. Phys.*, 2005, **7**, 3297–3305.
57 C. Angeli, R. Cimiraglia, S. Evangelisti, T. Leininger and J.-P. Malrieu, *J. Chem. Phys.*, 2001, **114**, 10252–10264.
58 C. Angeli, R. Cimiraglia and J.-P. Malrieu, *Chem. Phys. Lett.*, 2001, **350**, 297–305.
59 C. Angeli, R. Cimiraglia and J.-P. Malrieu, *J. Chem. Phys.*, 2002, **117**, 9138–9153.
60 I. Schapiro, K. Sivalingam and F. Neese, *J. Chem. Theory Comput.*, 2013, **9**, 3567–3580.
61 F. Weigend, M. Kattannek and R. Ahlrichs, *J. Chem. Phys.*, 2009, **130**, 164106.
62 S. Kossmann and F. Neese, *Chem. Phys. Lett.*, 2009, **481**, 240–243.
63 F. Weigend, *Phys. Chem. Chem. Phys.*, 2006, **8**, 1057–1065.
64 F. Neese, *Wiley Interdiscip. Rev.: Comput. Mol. Sci.*, 2022, **12**, e1606.
65 F. Neese, *Wiley Interdiscip. Rev.: Comput. Mol. Sci.*, 2018, **8**, e1327.
66 F. Neese, *Wiley Interdiscip. Rev.: Comput. Mol. Sci.*, 2012, **2**, 73–78.
67 G. Katzer, *Character Tables for Point Groups used in Chemistry*, **https://gernot-katzers-spice-pages.com/character_tables/index.html**.
68 J. R. Platt, *J. Chem. Phys.*, 1949, **17**, 484–495.